Performances of the JT-60SA cryogenic system in the integrated commissioning test

Kazuya Hamada[1*], Kazuma Fukui[1], Katsumi Kawano[1], Yoshihiro Onishi[1], Ryota Sakurai[1], Kiichi Ohtsu[1], Haruyuki Murakami[1], Katsuhiko Tsuchiya[1], Koji Takahashi[1], Sam Davis[2], Manfred Wanner[2], Valerio Tomarchio[2], Guy Phillips[2], Louis Zani[2], Isao Abe[3], Christine Hoa[3] and Frederic Michel[4]

[1] Naka Institute for Fusion Science and Technology, National Institutes for Quantum Science and Technology, 801-1 Muko-yama, Naka-shi, Ibaraki 311-0193, Japan
[2] Broader Approach & Roadmap Project Unit, Fusion for Energy, Boltzmannstr. 2 Garching bei München, Germany
[3] ITER organization, 13067 St. Paul-lez-Durance, France
[4] CEA - Universite Grenoble Alps, IRIG-DSBT, F-38000 Grenoble, France

[*]E-mail: hamada.kazuya@qst.go.jp

Abstract. A tokamak-type fusion experimental machine, JT-60SA, has been constructed through an international collaboration between Japan and the European Union. The JT-60SA utilizes a superconducting magnet system and a helium refrigerator with an equivalent refrigeration power of 9.5 kW at 4.5 K, providing cold helium gas to cool the magnet system. The second integrated commissioning test for JT-60SA operations began in May 2023, and the magnet system cooled down to operation temperature (<5 K). For plasma experiments, the cryogenic system provided approximately 2 kg/s of supercritical helium to the magnet system, removing static heat loads such as radiation and conduction heat and dynamic heat loads due to AC losses in the conductors, eddy currents in the magnet structures, and joule heating of the joints. The cryogenic system was successfully operated, and the first plasma was achieved on 23 October 2023.

1. Introduction

Toward an early realization of fusion energy, a Broader Approach (BA) Agreement between Japan and the European Union was established in 2007[1]. As part of this agreement, a tokamak-type fusion experimental device, JT-60SA, was constructed in Japan as a collaboration between Fusion for Energy and the National Institutes for Quantum Science and Technology (QST). JT-60SA uses a superconducting magnet system involving 18 Toroidal Field (TF) coils [2], 4 Central Solenoid (CS) modules, 6 Equilibrium Field (EF) coils, superconducting feeders, and 26 high-temperature superconductor (HTS) current leads [3,4] surrounded by an 80-K Thermal Shield (TS). The total cold weight is around 766 tons (TF: 396 tons, EF: 177.5 tons, CS: 100 tons, TS: 93 tons). A helium refrigerator system with an equivalent refrigeration capacity of 9.5 kW at 4.5 K [5] cools the magnet system, a thermal shield, HTS current leads, and refrigerates the Divertor Cryopumps [6,7]. The helium refrigerator system has been contributed by CEA (France) as an European in-kind contribution. The system was constructed by Air Liquide Advanced Technologies [8,9]. The assembly of JT-60SA tokamak was completed in March 2020, and the cool-down of the magnet system for the integrated commissioning (IC) of the entire system started in October 2020[10].

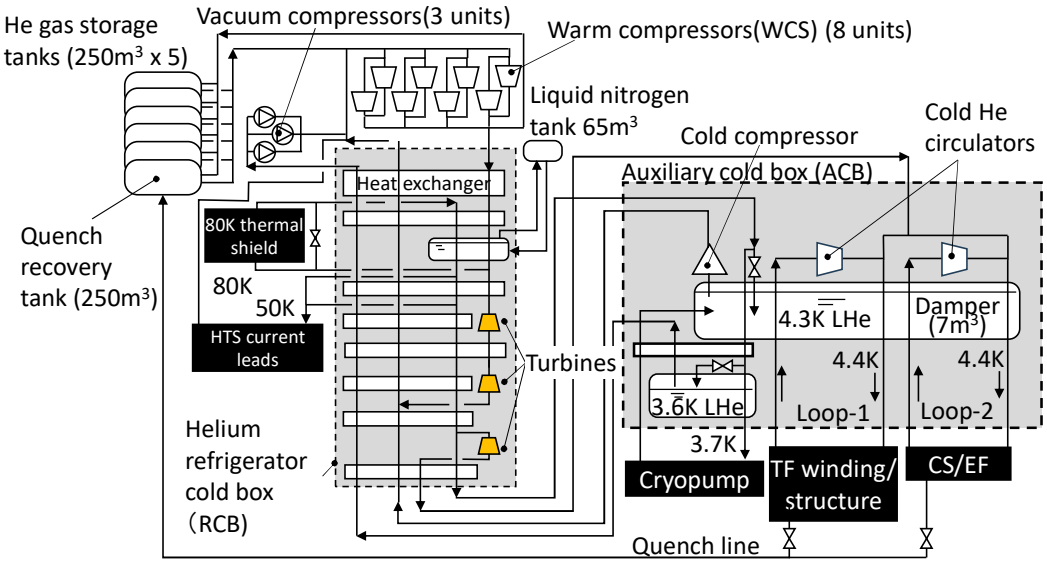

Figure 1. JT-60SA Cryogenic system process diagram.

However, the test was interrupted in March 2021 due to an electrical short at the electrical terminals of the EF1 coil [11]. From 2021 to 2023, repairs to terminals, electrical insulation reinforcement, and high-voltage tests were conducted. The IC was resumed in May 2023 [12]. In this paper, the outline of the cryogenic system and heat load profiles of the cryogenic system during cool-down and plasma experiments are reported.

2. Cryogenic system

The cryogenic system consists of a refrigerator cold box (RCB), an auxiliary cold box (ACB), eight units of warm compressor stations with a common oil removal system, helium gas buffer tanks, and utility systems (Figure 1). The RCB is equipped with three turbines and a pre-cooling system with liquid nitrogen. The warm compressor station provides pressurized helium of 0.7 kg/s at 1.4 MPaG. The RCB provides 5~6 K and 0.4 MPaG gas to be liquified in the ACB, 80 K for the TS [13], and 50 K for the 26 units of High-Temperature Superconductor (HTS) current leads. The ACB contains two liquid helium tanks used as a thermal damper system. The ACB supplies 2 kg/s supercritical helium (0.5 MPa, 4.4 K) to the magnet system using two cold circulators through a cryogenic piping system [14]. To maintain a liquid helium temperature of 4.3 K, the ACB has a cold compressor to reduce the vapour pressure in the 7 m³ liquid helium bath. CS and EF coils are operated with changing currents during plasma experiments to initiate and control the plasma, inducing variable heat loads by AC losses and eddy currents in the magnet structures. To mitigate the impact of transient heat fluctuations and ensure stable operation of compressors, turbine expanders, and cryogenic circulators, the 7-m³ liquid helium bath is used as a thermal damper system [8]. During a fast discharge of the magnet system, large eddy currents are induced. The released helium gas is recovered in the quench buffer tank to avoid helium gas exhaust to the atmosphere. A cryopump system behind the Divertor will be cooled with 3.7 K helium gas, which passes through a heat exchanger in a 3.6 K liquid helium tank. The helium in the 3.6 K bath is evacuated at -0.05 MPaG with a vacuum compressor system to reduce the saturated temperature. The cryopump system is being installed for future operation. As shown in Figure 2, there are two cooling loops. Magnet cooling Loop-1 is used for TF coils/structures, and Loop-2 is used for CS/EF

coils [14]. The two loops are composed of many parallel flow paths. The CS and EF have different pressure drop characteristics. Each TF coil has the same pressure drop characteristics. At nominal operation condition, the ACB supplies supercritical helium of 46~54 g/s for one TF coil, 156 g/s for one CS module, 56 g/s each for EF3, 5, 6, 48 g/s for each EF1 and EF2, 80 g/s for EF4, and 2 g/s for each feeder path [15].

3. Cool-down operation

3.1 Gas purification

Before starting a cool-down of the magnet system, the helium gas (total helium inventory: 2.9 tons) was purified. A dew point of less than -70 °C and a nitrogen content of less than 10 ppm in helium gas were achieved in 25 days by the following process.

(1) Circulating helium gas through a dryer installed in the outlet of the warm compressors,
(2) Repeating vacuum pumping and refilling with pure helium gas 5 times
(3) Circulating helium through the integrated molecular sieve adsorption purifier of the RCB.

The cryogenic system was operated for 7 months, including cool-down, magnet operation, and warm-up, and there was no trouble related to helium gas impurity.

3.2 Cool-down operation

During the cool-down operation down to 80 K, the helium was cooled with liquid nitrogen and sent from the RCB to the magnet system through ACB and to the TS. The flow distribution through the different coils was adjusted based on their weight ratio. After reaching 80 K, two turbine expanders were activated. Below 10 K, the third turbine was started to reach supercritical helium conditions. Finally, two cold circulators supply supercritical helium (4.3 K, 0.5 MPaG) to the magnet system. Since the TF coils, EF coils, and CS are mechanically interconnected, a total of 167 thermometers, as shown in Figure 2, were used to monitor the temperature differences to avoid

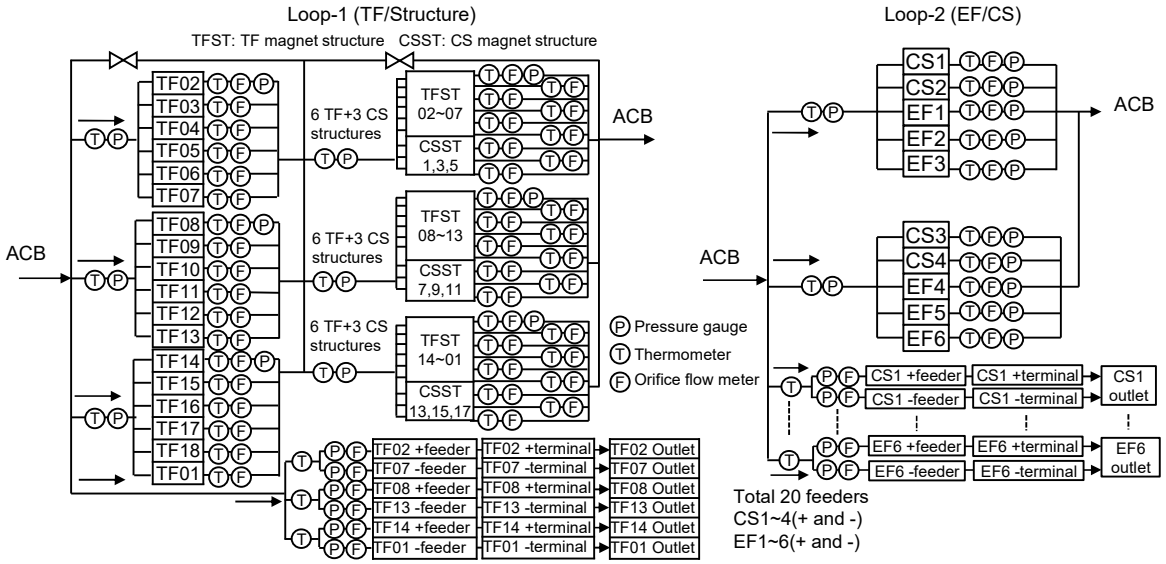

Figure 2. Flow diagram of Loop-1 and Loop-2.

damage by thermal stress within a coil and deformations due to the thermal contraction differences between the coils.

During the cooldown, the temperature difference was controlled based on the inlet and outlet temperatures of the coils, a thermometer on the surface of the coils, and the coil winding temperature calculated from the resistance measured by passing an electric current through the coil. The temperature change during the cooldown was 2 K/hr or less. The controlled temperature difference [16] is as follows.

- EF and TF coils: The cold helium is introduced from the innermost turn (high magnetic field region) and exits from a pancake's outer turn (joint). Since this temperature difference is the maximum temperature difference across the coil, the control value was set to 35 K.
- TF winding and coil structure: The winding is housed inside the TF coil structure. To avoid thermal stress on the windings during cooling, the temperature of the structure was kept 35 K or less above the winding.
- 18 TF coils: TF coils are connected in the circumferential direction by an Outer Intercoil Structure (OIS) with tension bolts to support out-of-plane forces [2]. The temperature difference between the TF coils is controlled within 10 K to avoid excessive force on the OIS by different TF coil temperatures. The TF coil temperature is estimated from the resistance of the TF winding.
- CS windings and CS structures [3]: The CS consists of four stacked modules. The CS is compressed by a CS structure (tie plate) made of stainless steel at room temperature to maintain compressive force after cooldown, and avoid separation of a module due to reaction forces during CS energization. To prevent the tie plate from shrinking and tightening the CS too much during the cooldown, and avoid overstressing the tie plate, the allowable temperature of the CS structure was kept 10 K or less above the winding temperature.
- CS winding: Since the helium is introduced from the cylindrical outer surface of the CS winding and exits from the cylindrical outer surface via the innermost part of the coil with a high magnetic field, the outlet temperature does not represent the maximum temperature in the coil due to heat exchange inside the coil. For this reason, the allowable temperature difference across the CS winding was evaluated based on analysis results [23], and the temperature difference of the helium between the inlet and outlet was set to 25 K or less.

3.3 Cool-down results

The second cool down started on 14 June 2023 [17]. The results for the magnet are shown in Figure 3. The cool-down was interrupted at around 100 K due to a grounding fault in the cold circulator controller. After the turbines started and the cooldown was continued, a 200 °C baking operation of the vacuum vessel started on 11th July. The cool-down operation was completed

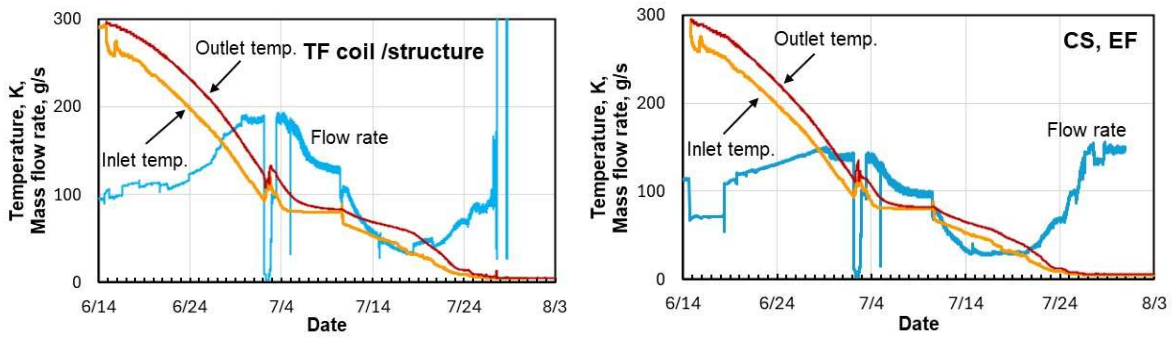

Figure 3. Cool-down curves of TF coil and structure (left) and CS and EF (right).

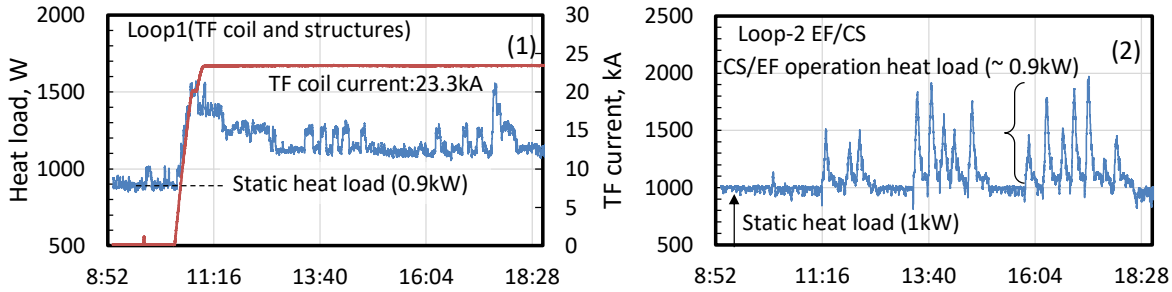

Figure 4. Typical example of heat load fluctuation for one day during plasma experiment[17].

when the superconducting magnet showed a transition to the superconducting state. It took 41 days. Except for the unplanned stop, the cool-down operation was smoothly completed.

4. Heat load and efficiency

4.1 Heat load variation during plasma experiment

During the plasma experiments, the TF coils were energized at a constant current (25.7 kA: nominal expected current for operation or 23.3 kA). AC losses were generated since the CS and EF coils were operated with varying currents to initiate the plasma current and control plasma position and shape. Figure 4 shows typical heat load fluctuations from morning to evening during the experiment day. The heat load is estimated from a mass flow rate and a difference between outlet and inlet enthalpies calculated from pressure and temperature measurement data. Due to the restriction of coil operation voltage, the maximum operation current of EF and CS was limited to 5 kA instead of a nominal current of 20 kA [16-18]. During the current ramp-up of the TF coil, the heat load increased due to AC losses of the TF coil and eddy currents in the case stabilizing again at the flat top of current. In the heat load of Loop-2 (Figure 4(2)), each peak corresponds to a plasma shot with CS and EF energization [17]. From Figure 4, the static heat load from radiation and thermal conduction can be estimated to be 0.9 kW for Loop-1 and 1 kW for Loop-2. Comparisons between prediction [19] and measurement of the TS and Loop-1 and 2 as summarized in Table 1, agree very well, so the thermal insulation worked as expected.

As shown in Figure 5, the total peak heat load of Loop-1 and Loop-2 is around 1.1~1.2 kW during the 5-kA operation of EF and CS. The cryogenic system and the 7-m^3 thermal damper have been designed to allow for the acceptance of about 5 kW pulse heat load. CS and EF coil currents will reach 20 kA during the next operation. If the current ramp-up and ramp-down are the same, AC loss will increase to roughly ~4.4 kW (=1.1 kW x 20 kA/5 kA). The value is still below 5 kW.

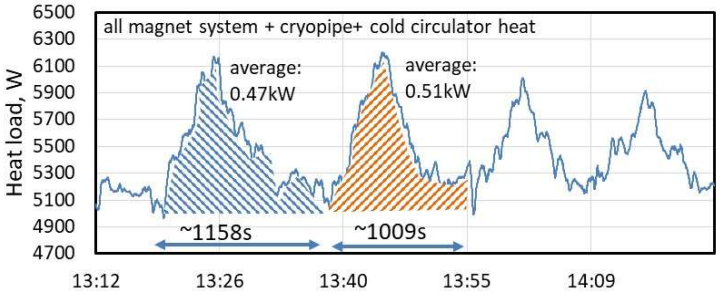

Figure 5. Typical total heat load fluctuation and averaged values of magnet system(Loop-1 and Loop-2) during one cycle of a plasma experiment (magnified from Figure 4).

Table 1. Prediction and measurement results of static heat load.

Static heat load	Estimation, kW [19]	Measured, kW
80K heat load (normal operation) (radiation and conduction)	Nominal: 33.1 (min. 28.3, max. 40.7)	32.5~35
4 K heat load (radiation and conduction)	Nominal: 1.5 (min. 1.18, max. 2.08)	1.9

In the IC, the averaged pulse heat load is only 0.5 kW, therefore, the heat load fluctuation did not have a significant impact on the operational condition of the warm compressor station and turbines.

4.2 Efficiency of cryogenic system

Based on Figure 4, we evaluated the heat load and efficiency of the refrigerator system during the plasma experiment (TF current: 23.3 kA, CS, EF: +/-5 kA), and the results are summarized in Figure 6. The total heat load of Loop-1 was 1.1 kW, which includes 0.2 kW of joule heating of the TF coil and feeder joints.

Adiabatic efficiencies of the turbines and cold circulators are around 70%. The adiabatic efficiency of the third-stage turbine and the cold compressor was lower than 50% because these rotating machines had not yet been operated at nominal conditions. As for the RCB, cold was supplied to the ACB, and 80 K helium gas at 0.38 kg/s was supplied to the 80 K shield. A total of 32.6 g/s of helium gas (44.6 K) was supplied to 26 units of the HTS current leads, which were finally recovered by the compressors at room temperature. The actual power consumption L of the compressor was measured at a distribution board and was 2.34 MW. The isothermal efficiency of the compressor is the ratio of the isothermal compression work to the actual power of the compressor. The isothermal compression efficiency $\boldsymbol{\eta_{is}}$was calculated using equation (1).

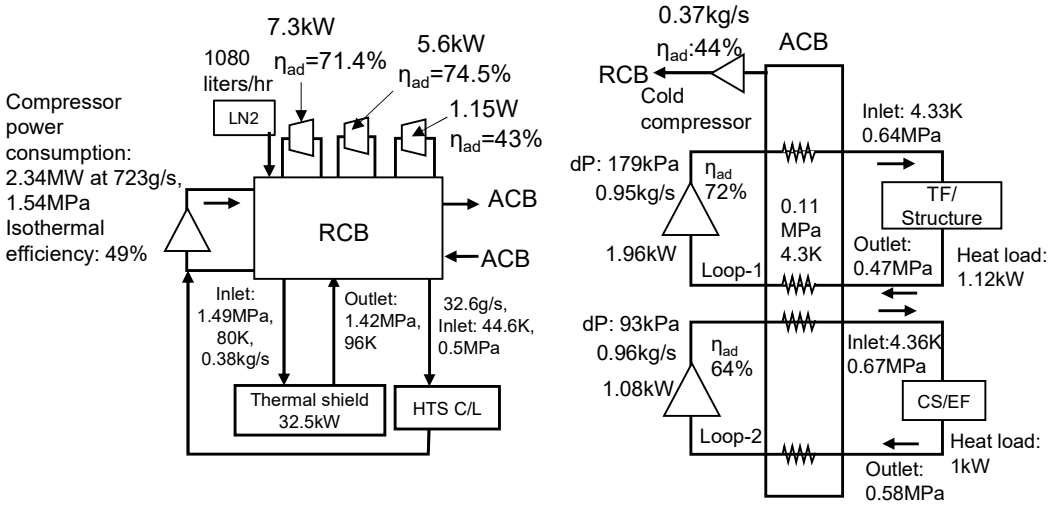

Figure 6. Typical cryogenic operation conditions, efficiency, and heat load during the plasma experiment at TF current of 23.3 kA.

Table 2. Total heat load during plasma experiment at TF coil current of 23.4 kA.

Items	Heat loads (kW)	Pin, (MPa)	Tin (K)	Pout (MPa)	Tout (K)	$\dot{m}$ (kg/s)	Exergy (kW)	Equivalent heat load at 4.5 K(kW)
Thermal shield at 80K	32.5	1.45	79.8	1.42	96.3	0.377	83.7	1.27
HTS current lead	42.1	0.56	44.7	0.43	293	0.033	59.0	0.90
Cold compressor	1.0	0.11	4.33	0.13	4.83	0.408	32.9	0.50
Damper dissipation (magnet heat loads + cold circulator)	5.16							4.92
Loop1 (TF/structure) heat load	1.12	0.638	4.33	0.466	4.8	0.954	151.1	2.30
Loop2 (CS/EF) heat load	1.00	0.667	4.33	0.578	4.68	1.07	109.7	1.67
Loop1 cold circulator work	1.96	0.461	4.35	0.647	4.68	0.954	42.7	0.65
Loop2 cold circulator work	1.08	0.571	4.33	0.671	4.48	1.07	19.8	0.30
TOTAL users equivalent heat load at 4.5K								7.60 kW

$$\eta_{is} = {}^{1}/_{L} \cdot R \cdot \dot{m} \cdot T \cdot ln({}^{P_{out}}/_{P_{in}}) \quad (1)$$

Here, R: gas constant (= 2.07 kJ/kgK), $\dot{m}$: flow rate (0.723 kg/s), T: inlet temperature (280 K), P_{in}: inlet pressure (0.106 MPa), P_{out}: outlet pressure (1.54 MPa), L: measured compressor power consumption(2.34 MW). The isothermal efficiency of the compressor station, including oil removal, is estimated to be 49%.

Since the JT-60SA refrigeration system supplies different refrigerants (4 K, 50 K, and 80 K), the input energy per 1 W of refrigeration capacity was evaluated by converting these refrigerants into an equivalent heat load of 4.5 K. The exergy was calculated from the pressure, temperature, and flow rate at the inlet and outlet of the cold compressor, cold circulator, coil, thermal shield, and current lead, and converted to an equivalent refrigeration capacity of 4.5 K using the Carnot factor [20].

$$e = \dot{m} \cdot \{(h_1 - h_2) - T_0 (S_1 - S_2)\} \cdot \frac{4.5}{300-4.5} \quad (2)$$

T_0: 300 K, h_1: enthalpy of exit, h_2: enthalpy of inlet, S_1: entropy of exit, S_2: entropy of inlet.

Table 2 summarizes the temperature, pressure, and flow rate at the inlet and outlet for each heat load and the calculation results. The equivalent refrigeration capacity of 4.5 K is 7.6 kW. The input electric power consists of the warm compressor station + utilities (~2.53 MW) and liquid nitrogen consumption. The realistic energy required to liquefy nitrogen is 0.5 kWh/kg [21]. The energy required to produce 1080 liters/hr of liquid nitrogen is 438 kW. The combined input energy of the compressor and liquid nitrogen is 2.97 MW. Therefore, the input energy per 1 W of refrigeration capacity at 4.5 K is 390 W. The typical input energy of a large-scale helium refrigerator is reported to be about ~300 W/W. The efficiency of the JT-60SA refrigerator is expected to improve when the refrigeration power approaches 9.5 kW during future operation.

5. Conclusion

The JT-60SA integrated commissioning test in 2023 was completed successfully.

- The cooldown of 28 superconducting coils was completed in 41 days under controlled temperature differences.

- The JT-60SA cryogenic system safely managed all heat load fluctuations.
- The measured static heat load of the cryogenic system is within expectation.
- No impurities in the helium gas nor any helium leak were observed.
- During 7 months of continuous operation, JT-60SA successfully achieved the first plasma and a maximum plasma current of 1.2 MA [22]. The experience gained with the cooldown and operation of the complex magnet system will help to improve future operations.

We would like to express our gratitude to Dr. Masaya Hanada, Director of the QST Naka Fusion Research Institute, Dr. Shunsuke Ide, Deputy Director, and Dr. Takahiro Suzuki, Director of the Advanced Tokamak Plasma Research Department. We would also like to thank the JT-60SA integrated project team, the JT-60SA magnet system group, and the cryogenic system operation team for cooperating in the integrated commissioning test.

JT-60SA was jointly constructed, funded, and exploited under the Broader Approach Agreement between Japan and EURATOM.

References

[1] Kamada Y et al. 2022 Completion of JT-60SA construction and contribution to ITER *Nucl. Fus.* **62** 042002
[2] Davis S et al. 2019 JT-60SA TF magnet assembly *Fusion Eng. Des.,* **146**, p 369
[3] Koide Y et al. 2015 JT-60SA superconducting magnet system *Nucl. Fus.* **55**, 086001
[4] Heller R et al. 2021 Overview and first operation of the high temperature superconductor current leads during integrated commissioning of JT-60SA *Fusion Eng. Des*. **172** 112910
[5] Hoa C et al. 2017 Installation and pre-commissioning of the cryogenic system of JT-60SA tokamak *IOP Conf. Ser.: Mater. Sci. Eng.* **171** 012047
[6] Michel F et al. 2012 Cryogenic requirements for the JT-60SA Tokamak *AIP Conf. Proc*. **1434** p 78
[7] Lamaison V et al. 2014 Conceptual design of the JT-60SA cryogenic system *AIP Conf. Proc.* **1573** p 337
[8] Hoa C et al. 2017 Performance of the JT-60SA cryogenic system under pulsed heat loads during acceptance tests *IOP Conf. Series: Mat. Sci. Eng*. **278** 012104
[9] Kamiya K et al. 2017 Commissioning of the JT-60SA helium refrigerator *J. Phys. Conf. Ser.* **897** 012015
[10] Michel F et al. 2022 Dynamic simulation of the first cool down of the JT-60SA cryo-magnet system *Cryogenics* **126** 103537
[11] Shirai H et al. 2024 Recent Progress of JT-60SA Project toward Plasma Operation *Nucl. Fus.* **64** 112008K.
[12] Hamada K et al. 2024 Lessons Learned From EF1 Electrical Short Incident During JT-60SA Integrated Commissioning Test *IEEE Tran. Appl. Supercond.* **34** 4200805
[13] Nakamura S et al. 2019 Design and manufacturing of thermal shield for JT-60SA *Fusion Eng. Des*. **146** p 2375
[14] Natsume K et al. 2019 Mechanical design of the JT-60SA cryogenic pipe system *Fusion Eng. Des.* **46B** p 2214
[15] Murakami H et al. 2019 Final Design of the Current Feeders and Coil Terminal Boxes for JT-60SA *IEEE Trans. Appl. Supercond*. **29** 420130
[16] Hamada K et al. 2024 Integrated commissioning test of JT-60SA magnet and Cryogenic system- Cryogenic System Operation Results *TEION KOGAKU* **59** p 289 (in Japanese)
[17] Hamada K et al. 2025 Superconducting magnet operation in JT-60SA integrated commissioning test *Fusion Eng. Des.* **215** 114946
[18] Murakami H et al. 2024 Energization results of JT-60SA poloidal field coil *TEION KOGAKU* **59** p 304 (in Japanese)
[19] Kamiya K et al. 2019 Summary of thermal analyses to determine the refrigeration power for the JT-60SA helium refrigerator *Cryogenics* **99** p 51
[20] Guy Gistau Baguer, 2020 *Cryogenic Helium Refrigeration for Middle and Large Powers* (Springer Cham)
[21] Gross R et al. 1994 Liquid hydrogen for Europe - the Linde plant at Ingolstadt *Linde Reports on Science and Technology* **54** p 37
[22] Takahashi K, JT-60SA IPT 2025 Achievement of first plasma and successful integrated commissioning in JT-60SA *Fusion Eng. Des*. **216** 115059
[23] Sonoda S et al. 2021 Effect of SHe temperature on cool-down speed in JT-60SA CS module *IEEE Trans. Appl. Supercond*. **31** 4201806